# Case Study: Visualization and Analysis of High Rayleigh number — 3D convection in the Earth's Mantle

Gordon Erlebacher[1] David A. Yuen[2] Fabien Dubuffet[2]

[1]School of Computational Science & Information Technology,
Florida State University, USA*

[2]Minnesota Supercomputer Institute, University of Minnesota, USA†

## Abstract

Data sets from large-scale simulations (up to $501^3$ grid points) of mantle convection are analyzed with volume rendering of the temperature field and a new critical point analysis of the velocity field. As the Rayleigh number $Ra$ is increased the thermal field develops increasingly thin plume-like structures along which heat is convected. These eventually break down and become turbulent. Visualization methods are used to distinguish between various models of heat conductivity and to develop an intuitive understanding of the structure of the flow.

**CR Categories:** I.3.3 [Computer Graphics]: Picture/Image Generation I.3.7 [Computer Graphics]: Three-Dimensional Graphics and Realism

**Keywords:** Mantle convection, plumes, volume rendering, unsteady flow, feature extraction, critical points

## 1 INTRODUCTION

Mantle convection is a problem of considerable interest in geophysical fluid dynamics, because of the richness in the physics such as variable properties, in particular the recent work which focusses on variable thermal conductivity [1]. Since the late 1980's mantle convection has been modelled in 3-D but at relatively low Rayleigh numbers like $10^5$ [2]. The resolution used at that time was relatively low, on the order of $2 \times 10^6$ grid points. Recently we have conducted high Rayleigh number calculations with close to $10^8$ grid points [3] Variable thermal conductivity introduces new nonlinearities into the temperature equation due to the presence of the square of the temperature gradient, which dominates over the Laplacian of the temperature. These nonliearities are more difficult to solve numerically and require higher spatial resolution than for constant thermal conductivity. The spatial structures of plumes associated with variable thermal conductivity are different from those of constant conductivity [4]. In this case study we extend our previous work on high Rayleigh number convection [5] to even higher Rayleigh numbers on the order of $10^9$ and consider alternative visualization tools and techniques to those used in our previous attempts to visualize mantle convection processes [6].

## 2 MATHEMATICAL MODEL

Mantle convection can be modelled as a fluid at infinite Prandtl number subject to the Boussinesq approximation. The motion of this fluid is solved for in a 3-D Cartesian geometry, with the vertical axis $(z)$ pointing downward (Figure 1). The equations of motion are the temperature equation with variable thermal conductivity,

$$\frac{DT}{Dt} = \nabla(\kappa(T,p)\nabla T)$$

and the momentum equation (which does not depend on the variable viscosity or conductivity)

$$\nabla^2 \mathbf{u} - \nabla p - R_a T e_z = 0,$$

$\frac{DT}{Dt}$ is the substantive derivative of temperature, $T$ is the deviation of temperature from a constant reference state, $\mathbf{u}$ is the velocity vector, $p$ is the pressure in excess of the hydrostatic value, $T$ is the temperature deviation from the background state, $R_a$ is the Rayleigh number and $e_z$ is the unit vector along the $z$ direction which is aligned with the gravity vector. The Rayleigh number $Ra = \alpha g \Delta T d^3/(\nu\kappa)$ where $\alpha$ is the thermal expansivity, $g$ is the gravitational acceleration, $\Delta T$ is the temperature drop across the mantle, $d$ is the depth of the mantle, $\nu$ is the kinematic viscosity and $\kappa$ is the surface value of the thermal diffusivity. As a result of variable conductivity, the terms on the right hand side of the temperature equation are non-linear functions of $T$ as opposed to the simple linear diffusion term in the constant conductivity case. Boundary conditions on temperature are $T = 0$ at $z = 0$ (cold top) and $T = 1$ at $z = 1$ (heated bottom). The dimensional temperature at the Earth's core-mantle boundary is uncertain and may range between 3200 K to 4500 K [7]. The physical domain has an aspect-ratio of $4 \times 4 \times 1$ for modelling 3-D mantle convection in a cartesian geometry. This geometric configuration has been used the past [8] to model dynamics of mantle convection at lower Rayleigh number than the ones considered here. The thermal mantle conductivity has two components, the radiative conductivity and the lattice conductivity. These expressions, given in [9, 10], are based on experimental phonon lifetimes and reflectance data.

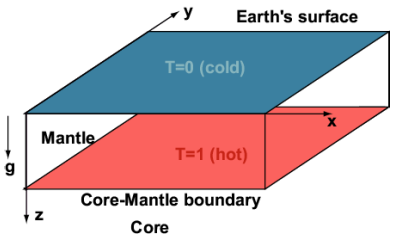


Figure 1: Geometry of mantle convection

*erlebach@csit.fsu.edu
†{davey,fabien}@msi.umn.edu

## 3 NUMERICAL METHOD

The flow is assumed to be periodic in the $x - y$ (horizontal) directions. The grid is uniform in all three directions. We have used an Alternating-Direction-Implicit scheme together with a finite difference method to solve the variable conductivity temperature equation. A Smolarkiewicz/finite-difference scheme is used for the constant conductivity case. The momentum equation is solved in the spectral domain using Fast Fourier Transform along the two horizontal directions and second-order finite-differences in $z$. Free-slip boundary conditions are imposed on the horizontal surfaces, while the vertical boundaries are impermeable.

Data from several simulations are used for this study. A low resolution $97^3$ simulation at $Ra = 10^6$ was chosen to illustrate the time-dependent nature of the data. These simulations (for constant and variable conductivity) were run for 8000 time steps, from which data at 300 time steps was stored and analyzed to study the time evolution of structural information. Two very high resolution simulations at $Ra = 10^8$ and $Ra = 10^9$ were conducted at resolutions of $401^3$ and $501^3$ grid points respectively. This data was generated for constant conductivity.

## 4 AMIRA

We have chosen the visualization package Amira [11] as the tool of choice for the display of complex flows. Similarly to AVS, Iris Explorer, and Data Explorer, Amira is based on interactive flowchart construction from a collection of predefined modules. Amira is built on top of Inventor, which provides facilities for high-level interaction with the data through embedded widgets. Many of the algorithms used in Amira make use of the hardware of current commodity graphics cards. As a result, Amira can manipulate very large data sets very efficiently. For example, it takes under 30 seconds to render a $400^3$ data set on a typical 1.7 GHz workstation with 1 Gbyte of memory. Amira is fully extensible through a well-defined object-oriented hierarchy of data structures that define grids and data types. Wrappers around many Inventor features are also provided. The algorithms discussed below have been implemented as Amira modules written by one of the authors. They are imported into Amira and appear as any other Amira module in the visual flowcharts.

## 5 THERMAL PLUMES

One of the fundamental challenges when analyzing flow turbulence is the identification of the so-called coherent structures. These have been defined in many ways, and to date there is still no real consensus. However, one definition that has appeal is to consider a coherent structure as a localized region of the flow that remains correlated over spatial and temporal scales much larger than the scales of the random flow component. Examples of such structures include turbulent spots in wall-bounded flow undergoing transition, hairpin vortices in wall-bounded turbulent flow, and elongated dissipative vortices in isotropic turbulence [12]. Such structures have been studied extensively, but aside from vortices, there have been very few algorithms developed to extract them. Feature extraction is seen as a necessary component required to successfully handle very large data sets in complex fluids.

When $Ra$ is sufficiently high, the temperature field develops turbulent characteristics, reminiscent of the turbulent velocity fields found at high Reynolds number. The coherent structures associated with the temperature field are called thermal plumes. They exist at lower Rayleigh numbers, but develop a range of spatial scales as $Ra$ is increased. Plumes play an important role in the dynamics of mantle convection because they determine the style of mantle convection and the global heat transfer. Until recently, the conductivity was assumed to be constant. The visualizations shown herein demonstrate that variable conductivity can change the spatial distribution and the strength of the plumes, thus affecting the dynamical processes through which heat is conducted through the mantle.

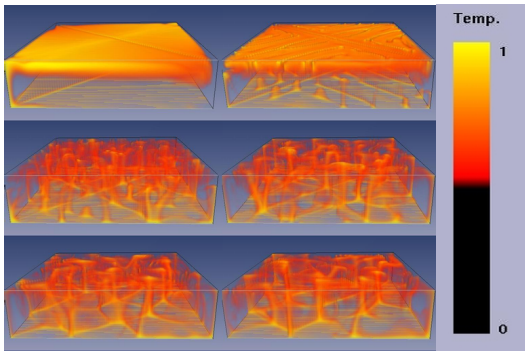


Figure 2: Plumes in $97^3$ dataset with constant conductivity. Six frames of an animation, equally spaced in time. The black regions of the color map correspond to 100% transparency.

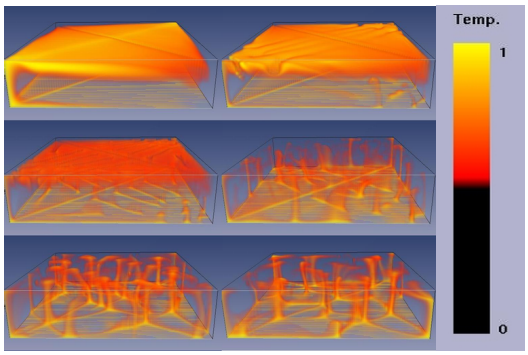


Figure 3: Plumes in $97^3$ dataset with variable conductivity. Six frames of an animation, equally spaced in time. The black regions of the color map correspond to 100% transparency.

Figures 2 and 3 are six frames taken from an animation of a volumetric representation of the temperature field at $Ra = 10^6$. The color map was chosen to emphasize the thermal plumes. (In its current version, Amira does not allow the transparent component of its color map to show. As result, the underlying color appears instead.) The first two images are at early time, the last two at times when the flow has become quasi-stationary. Comparing the constant and variable conductivity cases, we note that when the conductivity is constant, the plumes develop faster and their spatial density is higher. In both cases, the structure of the plumes is approximately constant: their height and shape don't vary much. On the heated plate (bottom), the temperature develops thin structures from which the plumes emanate. A better understanding of these structure is the focus of ongoing research. Qualitatively, the thermal plumes are tube-like; they are primarily vertical and extend from the bottom to the top plate.

As $Ra$ is increased further, the plumes become thinner and more irregular. When $Ra$ reaches the $10^7$ range, the temperature field becomes turbulent [5]. Figures 4 and 5 show the temperature field at a stage when the flow is quasi-stationary. The plumes have become more irregular, particularly at $Ra = 10^9$. Many plumes no longer extend throughout the mantle. To get a better idea of the structure of the plumes, $x - z$ and $x - y$ cross-sections are presented in Figures 6 and 7 respectively. The color maps correspond

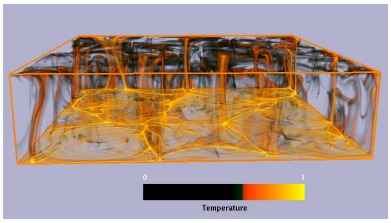


Figure 4: Volume rendering of a $401^3$ temperature field at $Ra = 10^8$ for a constant conductivity.

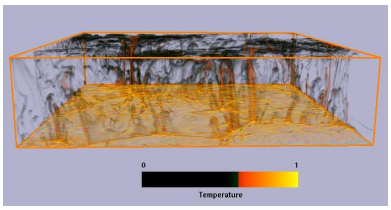


Figure 5: Volume rendering of a $501^3$ temperature field at $Ra = 10^9$ for a constant conductivity.

to those used in the volume-rendered images, including the transparency component (seen as black on the color maps). This choice of color map is meant to reduce accidental misinterpretation of the images when comparing plume slices and their 3-D representations. The top frame of each figure corresponds to $Ra = 10^8$, the bottom frame to $Ra = 10^9$. From the $x - z$ profiles, it is immediately apparent that the plumes are thinner at higher $Ra$. However, the thicker plumes are not immediately apparent from the $x - y$ cuts. What can be deduced through these visualizations is that the plumes originate from the heated plate at the intersections of the "canals" of local temperature maximum. These canals are conduits for the downswelling of colder fluid. The complex structure of the temperature field near the bottom plate at high $Ra$ is directly linked to the higher complexity of the plume structure.

From these images, we deduce that plumes under high Rayleigh number cover a very small fraction of the 3-D volume, which decreases further at higher $Ra$, although the plumes lose some of their identity. Thus the problem of visualizing and extracting plumes becomes more difficult at higher $Ra$. This would have been difficult to ascertain without the aid of advanced visualization software.

The next step is to develop techniques to extract these plumes and store them separately for analysis. Better understanding of their spatial distribution, their shape, and their volume would provide geoscientists with useful information to help their modelling efforts. However, it is not clear how to quantify a plume. The eye can clearly identify them from the 3D images, although the eye only sees an integrated intensity. On the other hand, planar cross-sections through the flow provide clear identification of these plumes. They indicate for example that the temperature gradient

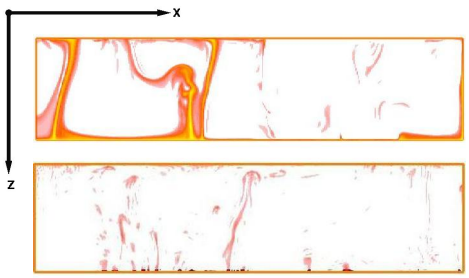


Figure 6: $x - z$ slice through the temperature field, chosen to capture a typical plume structure. Top: $Ra = 10^8$, bottom: $Ra = 10^9$. Constant conductivity. Flow is periodic in $x$ direction.

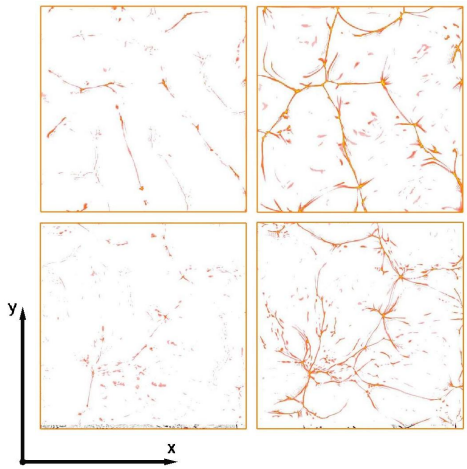


Figure 7: $x - y$ slices through the temperature field. Top: $Ra = 10^8$, slices 230 (left) and 386 (right) of 401 total. Bottom: $Ra = 10^9$, slices 388 (left) and 492 (right) of 501 total. Constant conductivity. Flow is periodic in $x$ and $y$ directions.

should play an important role in their identification. Unfortunately, both the temperature and its gradient vary along the plume edge (there are strong and weak plumes). Currently our color maps used by trial and error. Unfortunately, the color maps are not robust; a slight change in the mappings can easily make the plumes disappear, so automatic procedures are clearly required. We have developed a wavelet threshholding approach for plume identification. The color map would be generated based on field values in flow regions where the wavelet coefficients exceed a given threhhold. Unfortunately, the threshhold cannot yet be selected without user intervention.

## 6 VELOCITY FIELD

What is the relationship between the structure of the thermal plumes and that of the velocity field? The temperature field clearly indicates upswelling and downswelling motion between the bottom and top plates, but what is the precise mechanism by which this occurs? The temperature can vary either through thermal conduction, or by convection by the velocity field. Thus it is of some interest to better understand the time-evolution of the velocity field.

We explore a new use of critical points both as a means of flow representation in a highly compressed form and as a way to provide structural information about the flow. Critical points of the velocity field are intrinsically linked to the nonlinear dynamics of the flow [13]. In 3D flows, their structure provides clues regarding whether pathlines intersect planes along continuous curves or chaotic point distributions. In visualization, critical points have been used as a means of simplifying the representation of vector fields [14]. Critical points are the points in the flow where the velocity vanishes. The structure of the flow in a neighborhood of a critical point $\mathbf{x}$ is easily derived from the linear approximation to the vector field about $\mathbf{x}$. The type of the critical point is determined by the eigenvalues of the Jacobian of the velocity field evaluated at $\mathbf{x}$ is often used to characterize the nature of the flow (rotational, divergent, swirling, etc.). In three-dimensions, the structure of the flow in the neighborhood of a critical point is more difficult to interpret [15].

To date, critical points have not been exploited in time-dependent convective flows. The sparsity of critical points in 3-D flows leads us to consider an alternate technique that is meant to visualize the flow from the perspective of symmetry and global complexity. To accomplish this, we compute the critical points of three two-

dimensional flow fields $\mathbf{u}_z(x,y) = (u,v)$, $\mathbf{u}_x(y,z) = (v,w)$, and $\mathbf{u}_y(z,x) = (w,u)$. These fields are the 3D velocity restricted to the $x-y$, $x-z$ and $y-z$ planes. The subscripts $x, y, z$ remind us that these 2-D fields are parameterized by the third dimension. Next, we compute the critical points of $\mathbf{u}_z(x,y)$ in all $x-y$ slices and assign them a color. We do the same for the critical points in the $x-z$ and $y-z$ slices. Each critical point is displayed as a small cube. We precompute the critical points of the projected velocity fields that correspond to the 300 time slices of the $97^3$ data set at $Ra = 10^6$. We have found an average of 5000 critical points in each frame. The $Ra = 10^6$ dataset was chosen because it was cheap to recompute the flow and produce the required datasets. The flows at higher resolution were already computed and the data saved at much coarser time intervals.

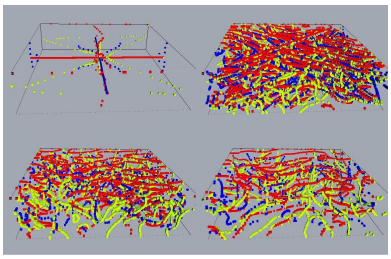

Figure 8: Four frames of an animation. Critical points of velocity fields projected on $x-y$, $x-z$ and $y-z$ planes. Constant Conductivity. $96^3$.

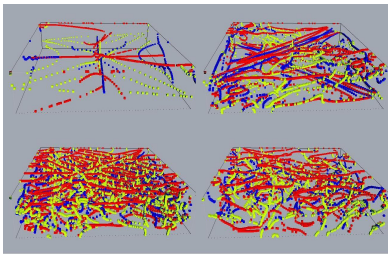

Figure 9: Four frames of an animation. Critical points of velocity fields projected on $x-y$, $x-z$ and $y-z$ planes. Constant Conductivity. $96^3$.

The results for the constant and variable conductivity data are shown in Figures 8-9 respectively. The top-left image corresponds to an early stage in the simulation, before the formation of the plumes. In the top-right image, the complexity of the flow has clearly increased, as determined by the number and more apparently random distribution of the critical points. Note, however, that the variable conductivity case maintains some structure for a longer time, consistent with the observations based on volume rendering of the temperature. The bottom-right image is representative of the state of the flow when it is quasi-stationary. We have constructed a module for Amira that can interactively browse through the critical points of all 300 sets data. The animation can be controlled by the software, or the user can interactively scan through the data for the purpose of exploration. Work is in progress to use this tool as a navigation device to zoom in on features of interest or to show alternate flow representations at the times selected by the user.

## 7 CONCLUSIONS

We have applied state-of-the-art visualization tools to some large-scale time-dependent mantle convection data sets to better understand the underlying structure of the temperature field, which becomes turbulent beyond a critical Rayleigh number. We have used the notion of critical points to construct a skeletal representation that helps characterize inherent symmetries and complexity in the flow. While volumetric rendering remains a fundamental tool to help understand the geometric structural intricacies of thermal plumes, there remains the task of developing robust algorithms for automatic color map generation and plume extraction. This work is fundamental to research activities Earthscope [16].

## References


[1] F. Dubuffet, D.A. Yuen, and M. Rabinowicz, "Effect of a realistic mantle thermal conductivity on the pattern of 3-d convection," *Earth Planet. Sci. Lett.*, vol. 171, pp. 401–409, 1999.

[2] D. Bercovici, G. Schubert, and G.A. Glatzmaier, "Three-dimensional spherical models of convection in the earth's mantle," *Science*, vol. 244, pp. 950–955, 1989.

[3] F. Dubuffet, D. A. Yuen, M. S. Murphy, E. O. Sevre, and L. Vecsey, "Secondary instabilities developed in upwellings at high rayleigh nubmer convection," in *EOS, TRANS, AGU*, 2001, vol. 82(47), p. F1210.

[4] F. Dubuffet and D. A. Yuen, "A thick pipe-like heat-transfer mechanism in the mantle: nonlinear coupling between 3-d convection and variable thermal conductivity," *Geophys. Res. Lett.*, vol. 27, no. 1, pp. 17–20, 2000.

[5] A.V. Malevsky and D.A. Yuen, "Plume structures in the hard turbulent regime of three-dimensional infinite prandtl number convection," *Geophys. Res. Lett.*, vol. 20, pp. 383–386, 1993.

[6] K.E. Jordan, D.A. Yuen, D.M. Reuteler, S. Zhang, and R. Haimes, "Parallel interactive visualization of 3d mantle convection," *IEEE Computational Science and Engineering*, vol. 3, no. 4, pp. 29–37, 1996.

[7] R. Boehler, "Melting temperature of the Earth's mantle and core: Earth's thermal structure," *Annu. Rev. Earth Planet. Sci.*, vol. 24, pp. 15–40, 1996.

[8] S. Balanchandar, D. A. Yuen, and D. Reuteler, "Time-dependent three-dimensional compressible convection with depth-dependent properties," *Geophys. Res. Lett.*, vol. 19, pp. 2247–2250, 1992.

[9] A. M. Hofmeister, "Mantle values of thermal conductivity and the geotherm from phonon lifetimes," *Science*, vol. 283, pp. 1699–1706, 1999.

[10] F. Dubuffet, D. A. Yuen, and S. G. Rainey, "Controlling thermal chaos in the mantle by positive feedback from radiative thermal conductivity," *Nonlinear Processes in Geophysics*, in Press, 2002.

[11] Template Graphics Software, "Home page," http://www.tgs.com.

[12] A. P. Vincent and M. Meneguzzi, "The dynamics of vorticity tubes in homogeneous turbulence," *J. Fluid Mechanics*, vol. 258, pp. 245–254, 1994.

[13] S. Lefschetz, *Differential Equations : Geometric theory*, Dover, 1977.

[14] J. Helman and L. Hesselink, "Surface representations of two- and three- dimensional fluid flow topology," in *Proceedings of IEEE Visualization*, 1990, pp. 36–46.

[15] A.E. Perry and M.S. Chong, "A description of eddying motions and flow patterns using critical-point concepts," *Ann. Rev. Fluid Mech.*, vol. 19, pp. 125–155, 1987.

[16] Earthscope, "Home page," http://www.earthscope.org.